Journal of Zhejiang University-SCIENCE A (Applied Physics & Engineering) *2024 25(6):483-501*
www.jzus.zju.edu.cn; www.springer.com/journal/11582
E-mail: jzus_a@zju.edu.cn

Research Article

https://doi.org/10.1631/jzus.A2300180

Deformation and stability of the seawall, considering the strength uncertainty of cement mixing piles

Yuansheng YU[1], Lingling LI[1], Xiangmiao KONG[3], Chengyuan LI[4], Zhen GUO[1,2]✉

[1]*Key Laboratory of Offshore Geotechnics and Material of Zhejiang Province, College of Civil Engineering and Architecture, Zhejiang University, Hangzhou 310058, China*
[2]*Hainan Institute, Zhejiang University, Sanya 572000, China*
[3]*Ninghai Highway and Transportation Management Center, Ningbo 315600, China*
[4]*Ninghai Traffic Engineering Construction Management Institute, Ningbo 315600, China*

Abstract: The cement mixing (CM) pile is a common method of improving soft offshore ground. The strength growth of CM piles under complex conditions is affected by many factors, especially the cement and moisture contents, and shows significant uncertainty. To investigate the stochasticity of the early strength of CM piles and its impact on the displacement and stability of a seawall, a series of laboratory tests and numerical analyses were carried out in this study. Vane shear tests were conducted on the cement-solidified soil to determine the relationships between the undrained shear strength s_u of the cement soil curing in the seawater and the cement content a_c, as well as the in situ soil moisture content w. It can be inferred that the 24 h undrained shear strength follows a normal distribution. A numerical model considering the random CM pile strength was established to investigate the deformation of the seawall. Due to the uncertainty of CM pile strength, the displacement of the seawall demonstrates a certain discreteness. The decrease of the mean undrained shear strength of CM piles causes a corresponding increase in the average displacement of the seawall. When the mean strength of CM piles is lower than a certain threshold, there is a risk of instability. Furthermore, the heterogeneity of the strength within an individual CM pile also has an impact on seawall displacement. Attention should be paid to the uncertainty of CM pile strength to control displacement and stability.

Key words: Construction uncertainty; Cement mixing (CM) pile; Strength of cement soil; Seawall stability; Random finite element method (RFEM); Monte Carlo simulation (MCS)

1 Introduction

Soil is a rather complex material that is influenced by geological deposition conditions, environmental factors, and physical-chemical effects. Non-negligible variability is apparent in its mechanical properties (Vanmarcke, 1977; Fenton and Griffiths, 2008). This phenomenon is particularly prominent in the coastal environment, and the uncertainty has become a severe challenge in offshore engineering practice, for example in bearing-capacity analysis, foundation settlement, and slope stability.

✉ Zhen GUO, nehzoug@163.com
Yuansheng YU, https://orcid.org/0009-0000-9777-2311
Zhen GUO, https://orcid.org/0000-0002-1869-8625

Received Apr. 6, 2023; Revision accepted July 31, 2023; Crosschecked Dec. 25, 2023; Online first Apr. 22, 2024

Lacasse and Nadim (1996) pointed out that the sources of uncertainty in predicting geotechnical response are generally categorized as either epistemic or aleatoric (der Kiureghian and Ditlevsen, 2009). Many related numerical studies and some physical models have been carried out to investigate this problem, as summarized in Table 1. Statistical analyses based on substantial amounts of data have been conducted to explore the effects of the spatial variability of soil properties on bearing capacity, foundation settlement, and slope stability. This spatial variability poses challenges for the design of the bearing capacity of a foundation and the stability of the slope. A design based on the determined properties of homogeneous soil will be on the unsafe side, as demonstrated by many studies.

The cement is used as a solidifying material in the construction of cement mixing (CM) piles, and can effectively improve the bearing capacity of offshore

Table 1 Numerical studies that consider the spatial variability of soil properties

Subject	Reference	Method	Parametric analysis	Main contribution and finding
Bearing capacity	Cassidy et al. (2013)	RFEM & MCS	COV	Failure envelopes under combined HVM loading
	Li JH et al. (2016)	RFEM & MCS	Correlation distance	Failure mechanisms and bearing capacity of a spudcan foundation
	Li et al. (2017a)	RFEM & MCS	COV	Distribution bearing capacity of a spudcan foundation
	Li et al. (2017b)	RFEM & MCS	–	Failure envelopes of spudcan with linearly increasing strength
	Wu YX et al. (2022)	RFEM & MCS	Horizontal correlation distance	Failure envelopes for various embedment depths and safety factor
	Wu CL et al. (2022)	Physical model	–	Physical model preparation and asymmetric failure mechanism
Foundation settlement	Griffiths and Fenton (2009)	SFEM, RFEM	Correlation distance	Comparison of SFEM and RFEM
	Jamshidi Chenari et al. (2019)	RFEM & MCS	COV, correlation distance, shallow foundation distance	Undrained settlement response of a pair of adjacent shallow foundations
Slope stability	Jiang et al. (2015)	MCS with subset simulation	–	Dealing with low probability levels by subset simulation and case study of layered cohesive slope
	Jiang and Huang (2016)	RSMs	–	Multiple stochastic response surfaces for representative slip surfaces (RSSs) in field with random c–φ
	Li DQ et al. (2016)	RSMs	–	Case study of layered cohesive slope and comparison of four commonly-used RSMs
	Zhu et al. (2017)	RFEM & MCS	Strength gradient, slope angle, correlation distance	Random field with linearly increasing strength with various gradients and various geometric parameters of the slope
	Hu et al. (2022)	RLEM & MCS	Slope angle, COV_c, $COV_{\tan\varphi}$	Categorization of failure modes with carious COV_c and $COV_{\tan\varphi}$, and calculation of stochastic sliding volume
Consolidation	Garzón et al. (2015)	Physical model, centrifuge test	–	Preparing nine homogeneous soils to construct heterogeneous models; mechanical properties dependent on location

RFEM: random finite element method; MCS: Monte Carlo simulation; SFEM: stochastic finite element method; RSM: response surface method; RLEM: random-limit equilibrium method; COV: coefficient of variance; COV_c: coefficient of variance for cohesion c; $COV_{\tan\varphi}$: coefficient of variance for $\tan\varphi$; φ: friction angle; HVM: horizontal, vertical, and moment

soft ground. The low price and simple construction method mean that this type of pile is widely applied in the field of geotechnical engineering (Nunez et al., 2013; Chai et al., 2015; Jamsawang et al., 2015; Lu and Miao, 2015).

The strength of CM piles is affected by many factors, such as cement content, in situ soil moisture content, curing environment, cementation time, organic matter content, and other construction factors. Strength growth under such complex conditions has significant uncertainty. Although some experimental studies have been performed on the solidification effect of cement on silt under various conditions (Kitazume et al., 2003; Kamruzzaman, 2009; Horpibulsk et al., 2011), most of them focus on the strength resulting from a long curing time (≥7 d), while there is relatively little research on the early strength development of solidified soil. However, the time interval between ground improvement and subsequent structure construction is not long enough to ensure full development of the strength of CM piles, so it is difficult to provide a theoretical reference or a design basis for this scenario. In addition, the above uncertainty analyses based on the random finite element method (RFEM) and Monte Carlo simulation (MCS) were focused only on the inherent spatial variability of the soil, and few studies

consider the uncertainties caused by the strength variability of CM piles. Thus, it becomes even more difficult to provide a reliability evaluation for in-field practice applying CM piles.

This paper proposes an analysis method for investigating the deformation and stability of a seawall, taking into consideration the uncertainty of the strength of the CM piles (based on laboratory tests on the cement-solidified soil). A vane shear test was carried out first to study the early strength development of the cement-solidified soil curing in the seawater within the first 24 h, considering the cement content a_c and the in situ soil moisture content w as variables. Based on the data obtained from the test, it is assumed that the in situ soil moisture content and cement content follow the normal distribution, and the probability distribution function (PDF) of the cement soil strength can be obtained by Monte Carlo sampling and bilinear interpolation. Finally, an RFEM model for the sand-filled embankment with a USDFLD subroutine to assign the random strength to the CM piles is established. The deformation of the seawall and the ground soil with variance pile strengths is calculated and analyzed statistically to evaluate the influence of the construction uncertainty of the CM piles on the deformation of the structure. On the basis of the proposed model, a further discussion is carried out, leading to a deeper and broader reliability analysis. This study will help to pave the way for a reasonable uncertainty analysis method and a reliable design for soft ground improvement using CM piles in offshore engineering practice.

2 Early strength of cement-solidified soil

2.1 Test set-up and method

In this test, in situ soil taken from Xidian, Ninghai, China (121.44° E, 29.46° N) was used to prepare the cement-solidified soil. Its basic mechanical properties were determined by geotechnical laboratory tests, referring to ASTM D854-14, ASTM D4318-17, ASTM D2216-19, and ASTM D7263-21 (ASTM, 2014, 2018, 2019, 2021), as presented in Table 2. The microstructure of the in situ soil is shown in Fig. 1. The smaller particles show an obvious lamellar structure and adhere to the larger particles. The edge-to-face connection and the phenomenon of overhead are evident, and result in high compressibility of the in situ soil.

Table 2 Basic mechanical properties of the in situ soil (silt layer)

Parameter	Value
Specific gravity, G_s	2.74
Moisture content, w (%)	61.6
Unit weight, γ (kN/m^3)	16.7
Void ratio, e_0	1.732
Liquid limit, w_L (%)	47.4
Plastic limit, w_P (%)	25.8
Liquid index, I_L	1.63

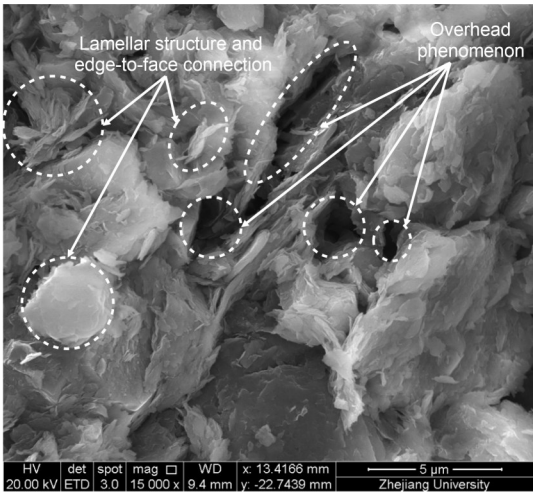

Fig. 1 Microstructure of the in situ soil under 15000-time magnification

The cement used for the test was PO42.5 ordinary Portland cement. To simulate the environment in which the CM piles were constructed and supported a certain seawall, the fresh water was used to prepare the cement soil samples, and the samples were immersed in seawater. The seawater used in the test was taken from Zhoushan, China. According to the test, the pH of the seawater was about 7.81, which is weakly alkaline. The main ion components and contents of the seawater are displayed in Table 3. The geological locations of the sampling sites and Xidian Bay are given in Fig. 2.

Table 3 Contents of the main ions in seawater used in the test

Ion	Content (mg/L)	Ion	Content (mg/L)
Cl^-	15005.3	Mg^{2+}	1610.7
Br^-	12.1	K^+	246.5
SO_4^{2-}	2302.9	Ca^{2+}	424.3
Na^+	7890.5		

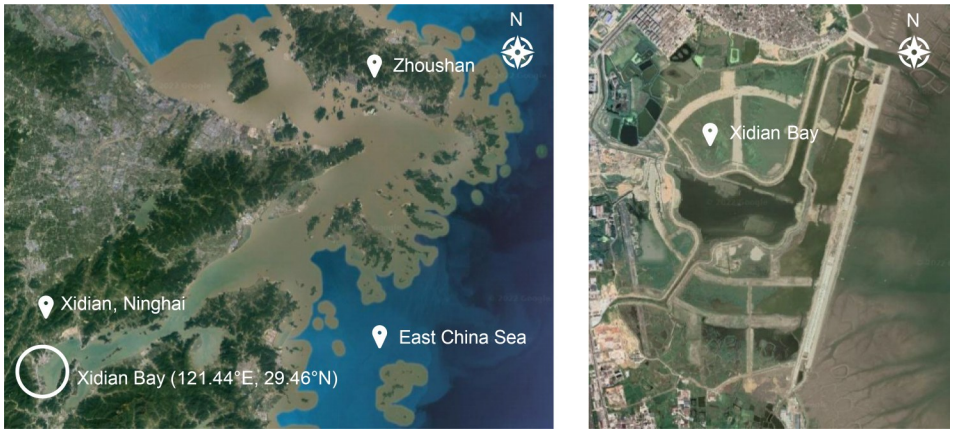

Fig. 2 Geological locations of the sampling sites and Xidian Bay

The undrained shear strength s_u of the cement soil within 24 h was determined by a vane shear test, referring to ASTM D4648M-16 (ASTM, 2016). During the test, the vane shear rate was controlled by the servo motor to be 0.15 (°)/s, to meet the standard requirements. The total range of the torque meter was 5 Nm, and the accuracy was 0.1%. The conversion formula between the torque and undrained shear strength is

$$s_u = \frac{2M}{\pi d^2 (h + d/3)}, \tag{1}$$

where M is the torque measured in the test, and h and d are the height and diameter of the vane, respectively. In this test, h=32 mm and d=16 mm.

A plexiglass cylindrical mold with a total height of 183 mm, an outer diameter of 100 mm, a wall thickness of 2 mm, and a bottom plate thickness of 3 mm was used for the test. According to the numerical analysis, when the height of a cement soil sample is $H \geqslant 5h$=160 mm and the diameter of the sample is $D \geqslant 6d$= 96 mm, the influence of the boundary effect can be eliminated. Thirty-three through-holes with a diameter of 3 mm were on the bottom plate of the mold so that the seawater could effectively contact the bottom surface of the sample.

This study focused on the influence of the in situ soil moisture content w and cement content a_c during construction on the early strength of the CM piles. The values of the moisture content w were set as 55%, 60%, 65%, 70%, and 75%, and the values of the cement content a_c (the ratio of the mass of cement added to the wet mass of the reinforced soil) were set as 8%, 11%, 14%, 17%, and 20%. Taking the unsolidified soil of any quality to prepare the cement soil sample by a given (a_c, w), the required quality of cement and seawater is calculated as follows:

$$m_c = \frac{1+w}{1+w_0} a_c m_0, \tag{2}$$

$$m_w = \left(\frac{w - w_0}{1+w} + \mu_c a_c \right) \frac{1+w}{1+w_0} m_0, \tag{3}$$

where m_0 is the mass of the dried soil; w_0 is the moisture content of the untreated soil, which was measured and updated every 2 d; m_c is the mass of required cement; m_w is the mass of required seawater; μ_c is the water-cement ratio (the ratio of water to cement mass in the cement slurry), which is taken as 0.7 here.

In the test, the wetted geotextile and the filter paper were first laid on the bottom of the mold to prevent the cement soil from flowing out through the bottom opening, and to ensure that the seawater could contact and penetrate the bottom surface of the sample. We mixed the unsolidified soil, cement, and seawater according to the mixing ratio, and then poured them into the mold in 4–6 layers until the cement soil filled the mold. After each filling with cement soil, we used a thin rod to pound the soil and shake it evenly to eliminate the large volume of air bubbles and pores. We scraped the upper surface of the sample and put the mold into the seawater. Small iron blocks were used to elevate the bottom of the mold and the whole mold was immersed in the seawater. The procedure for sample preparation is shown in Fig. 3. The undrained shear strength of the cement soil samples was measured at 2 h, 4 h, 7 h, 10 h, and 24 h. A total of

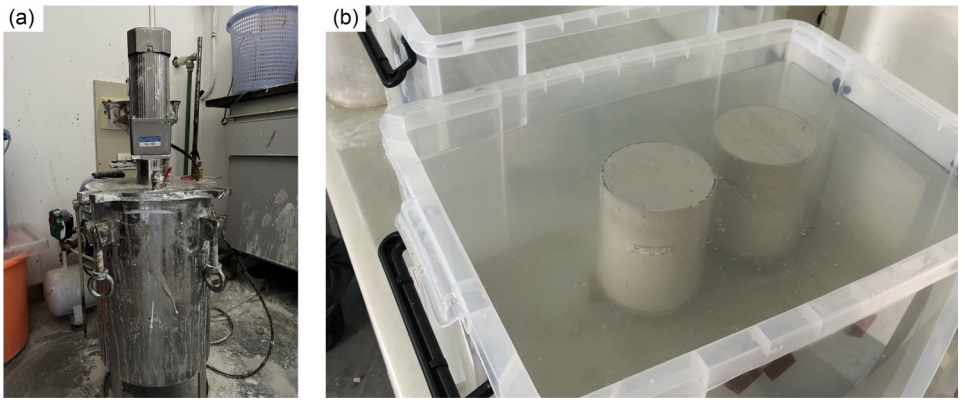

Fig. 3 Sample preparation: (a) mixed under vacuum condition; (b) immersed in seawater

125 samples were prepared according to different cement contents and moisture contents.

2.2 Test results and analysis

Taking the 24 h test results as an example, the test results of undrained shear strength of the cement soil are shown in Fig. 4a. Within the same curing time, the undrained shear strength of cement soil generally increased with an increase in cement content a_c, but decreased with an increase in in situ soil moisture content w. When the in situ moisture content was 75% and the cement content was 8%, the strength of the cement soil was only 51.36 kPa; when the cement content was 20%, the strength was 150.15 kPa. When the in situ moisture content was 55% and the cement content was 8%, the cement soil strength was about 135.23 kPa; when the cement content was 20%, the cement soil strength reached 235.45 kPa. Therefore, it was evident that the in situ soil moisture content and cement content had a significant effect on the strength of solidified soil.

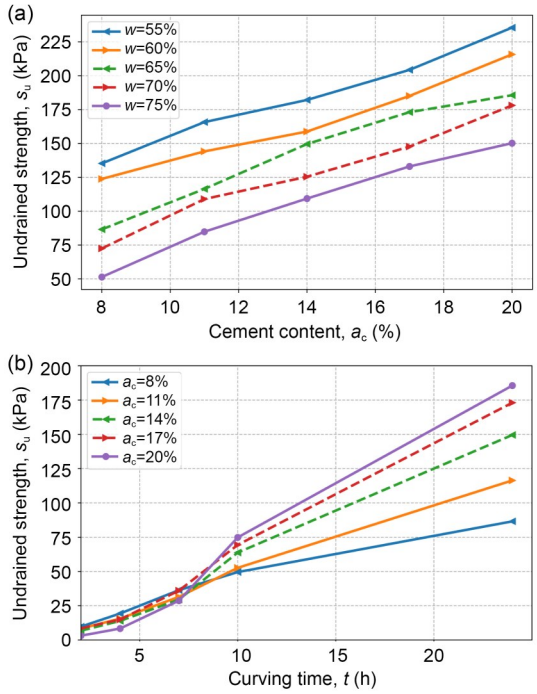

Fig. 4 Short-term undrained shear strength of the cement soil: (a) s_u–a_c with curing time t=24 h; (b) s_u–t with w=65%

Within the curing time of this test (24 h), the undrained shear strength of the solidified soil increased significantly with curing time, as seen in Fig. 4b. This can be attributed to the stronger cementation between particles. In addition, as hydration progressed, the pore water inside the solidified soil decreased due to the reaction, and the soil moisture content decreased, thus significantly enhancing soil strength.

3 Monte Carlo sampling and interpolation

3.1 Sampling method

The Monte Carlo method was first proposed by Metropolis and Ulam (1949). It is a general type of probability-based method that uses random numbers to solve statistical computing problems and obtain the real value or distribution through continuous sampling and approximation.

In situ soil moisture content is an inherent property of the soil, while the cement content added during construction is a variable caused by human factors. Therefore, there is no significant correlation between the two. In other words, changes in cement content during construction are not caused by the uncertainty of the in situ soil moisture content. Therefore,

we assumed that the in situ soil moisture content w and cement content a_c during the construction of the CM piles were random variables that would follow the normal distribution. The parameters of the normal distribution are included in Table 4. The probability density distribution curve shown in Fig. 5 was obtained by random sampling. Since there were upper and lower boundaries for the in situ soil moisture content and cement content in the vane shear test, the sampling results were limited in advance to ensure the feasibility and correctness of the interpolation algorithm.

Table 4 Normal distribution parameters of in situ soil moisture content w and cement content a_c

Random variable	Mean value, μ	Standard deviation, σ	COV
In situ soil moisture content, w (%)	65	6.5	0.1
Cement content, a_c (%)	14	4.2	0.3

These two random variables were independent of each other in this study, because there was no significant correlation between in situ soil moisture content and cement content during construction. Therefore, it was only necessary to randomly pair the sampling results to obtain the results shown in Fig. 6.

3.2 2D interpolation and results

In practice, after the completion of CM pile construction, a construction interval is often required to ensure that the cementation between the cement and the soil has taken place, and that a certain amount of strength has developed in the CM piles. Based on the conservative principle, we assumed for the purposes of this study that the seawall would be filled within 24 h after construction of the ground improvement, so the vane shear test results of the solidified soil at 24 h are taken. The 2D interpolation was performed by determining the four test-data points near the sampling point to be interpolated.

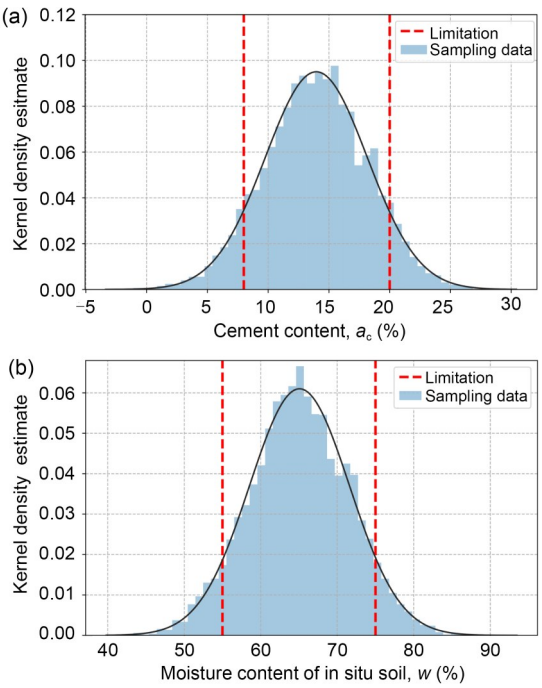

Fig. 5 Sampling results of the normal distribution of the cement content (a) and moisture content of the in situ soil (b). Dashed lines correspond to the upper and lower limits of cement content and in situ soil moisture content in tests

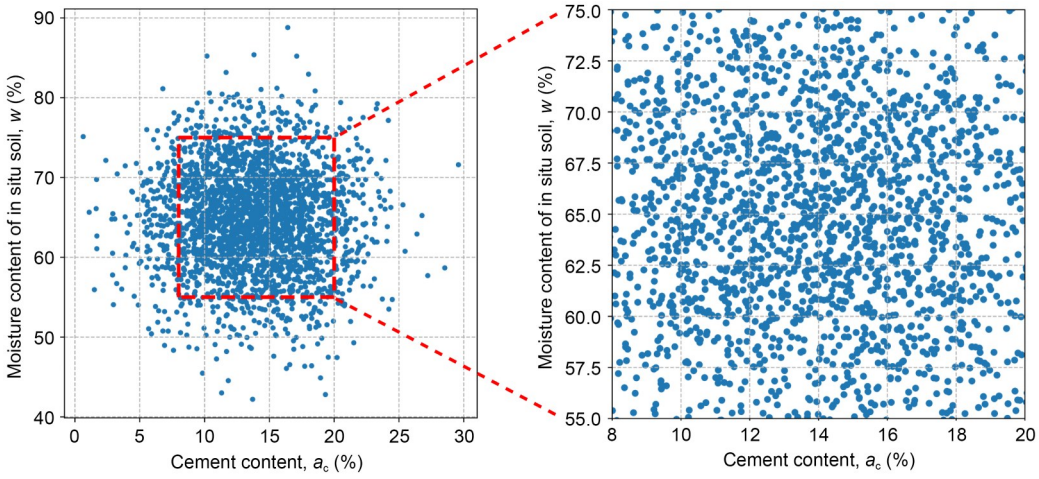

Fig. 6 Scatter plot of Monte Carlo sampling. The scatter points represent the possible states of the cement soil during construction, and the density of the scatter points reflects the occurring probability of the states

A bilinear interpolation algorithm (Kirkland, 2010) was used, and the calculation diagram is presented in Fig. 7. First, the linear interpolation was performed in the direction of the a_c axis to obtain the coordinates of the triangle marking points (a_c, w_1) and (a_c, w_2).

$$s(a_c, w_1) \approx \frac{a_{c,2}-a_c}{a_{c,2}-a_{c,1}} s_{11} + \frac{a_c-a_{c,1}}{a_{c,2}-a_{c,1}} s_{21}, \quad (4)$$

$$s(a_c, w_2) \approx \frac{a_{c,2}-a_c}{a_{c,2}-a_{c,1}} s_{12} + \frac{a_c-a_{c,1}}{a_{c,2}-a_{c,1}} s_{22}, \quad (5)$$

where s_{11}, s_{12}, s_{21}, and s_{22} stand for the undrained shear strengths at points $(a_{c,1}, w_1)$, $(a_{c,1}, w_2)$, $(a_{c,2}, w_1)$, and $(a_{c,2}, w_2)$, respectively.

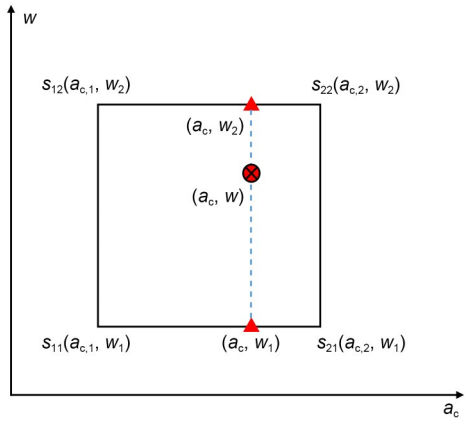

Fig. 7 Calculation diagram of the bilinear interpolation. The circle marking point with a cross represents the point to be interpolated

Then, we performed linear interpolation in the direction of the w axis to obtain the undrained shear strength $s(a_c, w)$ at the point (a_c, w):

$$s(a_c, w) \approx \frac{w_2-w}{w_2-w_1} s(a_c, w_1) + \frac{w-w_1}{w_2-w_1} s(a_c, w_2). \quad (6)$$

The curve in Fig. 8 indicates the probability density distribution function of the undrained shear strength of the pile body after sampling and 2D linear interpolation of 104 times. If the distribution is assumed to be a normal distribution, according to the central limit theorem, one can calculate that the mean value μ of the 104 samples is 144.27 kPa, and the standard variance σ is 30.46 kPa. The Kolmogorov-Smirnov (K-S) test results showed that the p-value was 0.185>0.05, so the assumption could be accepted.

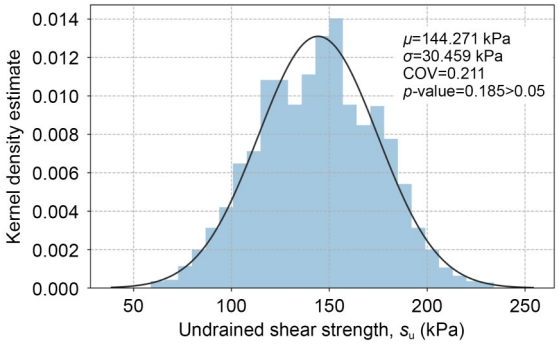

Fig. 8 Probability density distribution of the undrained shear strength of CM piles

According to the above results, in the following numerical study, the undrained shear strength of the cement soil should follow a normal distribution with μ=144.27 kPa and COV=0.211.

4 Deformation analysis incorporating the strength uncertainty of CM piles

4.1 RFEM model

The total length of the seawall at Xidian Bay is about 2.28 km, as shown in Fig. 9a, and the stratum of the construction area is marine tidal-flat sediment. The shallow soil mainly consists of silt, sandy silt, and gravelly silt clay. The soft soil layer is uneven in

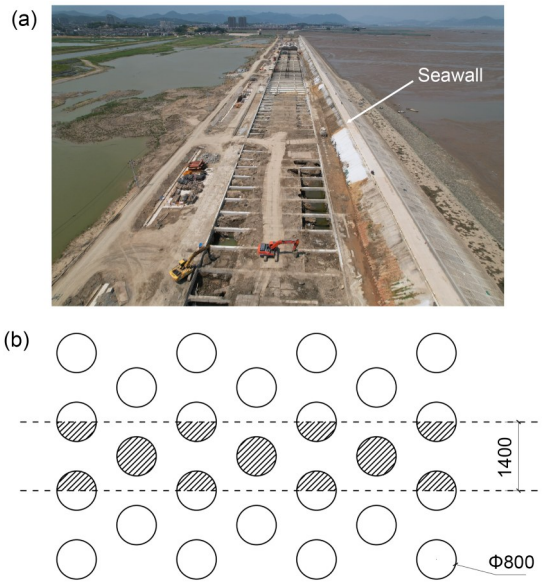

Fig. 9 (a) Panoramic view of the project; (b) schematic diagram of the CM pile layout under the seawall and the chosen width of the RFEM model (unit: mm)

thickness and exhibits a high pore ratio, high water content, high compressibility, low strength, and slow consolidation. To increase the bearing capacity of the soft ground, the CM piles were therefore introduced beforehand at the seawall construction area.

In this study, a random finite element numerical model in ABAQUS that took into consideration the random shear strength of the CM piles was established. As shown in Fig. 9b, the CM piles below the seawall followed a plum-shaped arrangement, with a diameter of 800 mm and spacing of 1.4 m. Based on this symmetry, we took a 1.4-m width along the longitudinal direction of the seawall as the unit of numerical analysis, and a total of 46 CM piles are included.

Fig. 10 illustrates the modeling of the ground soil (with the CM piles) and the seawall to represent a typical section. The scale of the ground soil is 200 m× 1.4 m×21.5 m, which is divided into two layers. The shallow layer is the silt, and the distribution range is from 0 m to −8.0 m, while the deeper layer is the gravelly silt clay, and the distribution range is from −8.0 m to −21.5 m. The elevation of the end of the CM piles is −8.0 m. The seawall is filled with geomembrane bags containing sand. The top elevation of the seawall is 8.8 m, and the slope of its inner foot is about 1:1.2. The outer foot is reinforced by the overload suppression, and the top elevation is 3.5 m.

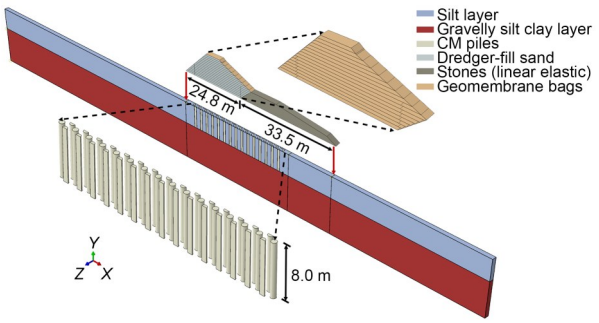

Fig. 10 Development of the finite element model. References to color refer to the online version of this figure

The 3D solid parts in the numerical model were all simulated by the C3D8R element. Soils were simulated with a Mohr-Coulomb elastoplastic model, and the material parameters are shown in Table 5. The strength of silt at the surface c_s=13.8 kPa, the friction angle φ=4.1°, and the undrained shear strength $s_u(z)$ was calculated according to the self-weight stress. The undrained shear strength of the CM piles was determined by the field variable, and the relationship between the elastic modulus and the undrained shear strength was assumed to be linear (Liu et al., 2015; Li et al., 2017b). Due to the adoption of the undrained analysis method, Poisson's ratio of the soil is set to 0.49. The geomembrane bag in the seawall was simplified as a linear elastic material, and the S4R element was used to simulate it. The weight of the geomembrane bag material was ignored; the thickness of the single-layer membrane bag was 5 mm; the elastic modulus was 80 MPa, and there would be no in-plane compressive stress on the geomembrane bag.

The contact between the structures was simplified to a certain extent. The relative displacement between the CM piles and the soil was ignored because there was also a cementing effect on the soil around the piles. Meanwhile, the relative displacement between the geomembrane bags was very small due to the large mass of the sand in each geomembrane bag and the rough surface of the bag, which was no longer considered in the numerical model. Only the contact between the seawall and the ground soil was covered in the analysis. The tangential friction coefficient was 0.36, and the normal direction was set as hard contact.

As seen in Fig. 9a, the proposed numerical model can be considered carrying out under a plane-strain case. Thus, the bottom of the numerical model was fixed in all three directions, while at the side of the model, no horizontal deformation was permitted. The surface of the ground and the upper surface of the

Table 5 Material parameters of soil and cement pile (Mohr-Coulomb model)

Item	Unit weight, γ (kN/m^3)	Young's modulus, E (kN/m^2)	Poisson's ratio, v	Cohesion, c (kPa)	Friction angle, φ (°)	Undrained shear strength, s_u (kPa)
Silt	16.70	3.32×10^3	0.49	–	–	$13.8+\gamma z\tan\varphi$
Gravelly silt clay	19.30	22.44×10^3	0.49	24.0	12.6	–
Dredger-fill sand	20.00	14.86×10^3	0.49	4.0	28.0	–
Cement soil	18.00	$250s_u$	0.49	–	–	Determined by field variables

z: depth of the soil

seawall were free boundaries. The gravitational acceleration of the seawall was 0 during the geo-balance step, and a gravitational acceleration of −10 m/s^2 was given in the filling step to simulate construction of the seawall under undrained conditions.

The global mesh size of the numerical model was set to be 0.5 m, while the mesh size of the seawall, ground soil below the seawall, and the CM piles was 0.2 m. For the area distant from the seawall, the mesh size increased with distance. The seawall and ground soil were meshed into 64988 and 79464 cells, respectively. A schematic diagram of the grid division is depicted in Fig. 11.

The state variable STATEV(1) was first differentiated in the keywords of the numerical model: STATEV(1)=0 for in situ soil and STATEV(1)=1–46 for soil within a CM pile. We used the USDFLD subroutine (ABAQUS Inc., 2016) to assign a linearly increasing strength with depth to the in situ soil, and to modify the soil's material properties within the CM piles in different analysis steps. This subroutine allows users to define field variables at a material point as functions of time or of any of the available material-point quantities listed in the output variable and update the state variables. During the geo-balance step, the material parameters of the soil in this range were still the same as those of in situ soil, and in the filling step, they were replaced by the parameters of the cement soil. A randomly generated strength value was assigned to each CM pile at the same time, based on the state variable. The subroutine controlled the values of two field variables. The mapping rule between the strength and the field variable was s_u=FIELD(1), and the values of FIELD(2) controlled the weight and elastic modulus of the soil in the range of the CM piles in different analysis steps. Figs. 12 and 13 show the algorithm and its effect, respectively.

4.2 Results with deterministic pile strength

To clarify the deformation pattern of the seawall and the ground soil, and the development of the plastic region (considering the CM piles and geomembrane bags), the calculation should first be carried out with the uniform pile strength. The undrained shear strength s_u of the CM piles was taken as 70 kPa, and Young's modulus was taken as E=500s_u=35.0 MPa.

Fig. 14 presents the horizontal and vertical displacements of the seawall and ground soil. Based on the calculation result, the deformation pattern was characterized as significant settlement at the top and a certain degree of uplift at the foot, as well as lateral deformation towards the inner side of the seawall due to horizontal compression. The maximum settlement of the top of the seawall was about 23.35 cm, and the uplift of the inner foot was about 11.47 cm. Due to the ground improvement with the CM piles, the settlement of the ground soil beneath the seawall was relatively small and uniform. The maximum settlement was about 17.08 cm directly beneath the top of the seawall. The horizontal displacement of the inner foot of the seawall was about 23.12 cm, while the horizontal displacement and the uplift of the outer foot were significantly suppressed due to the overload.

One can see from Fig. 15, which illustrates the distribution of the maximum plastic principal strain of the seawall and the ground soil, that the plastic strain developed mainly at the bottom of the seawall and in the silt layer. There were obliquely crossed shear zones

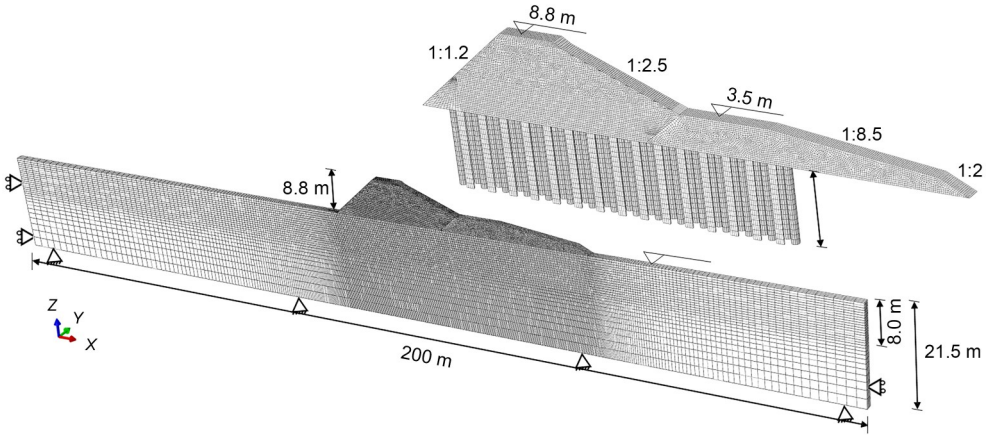

Fig. 11 Geometry, mesh, and boundary conditions of the finite element model

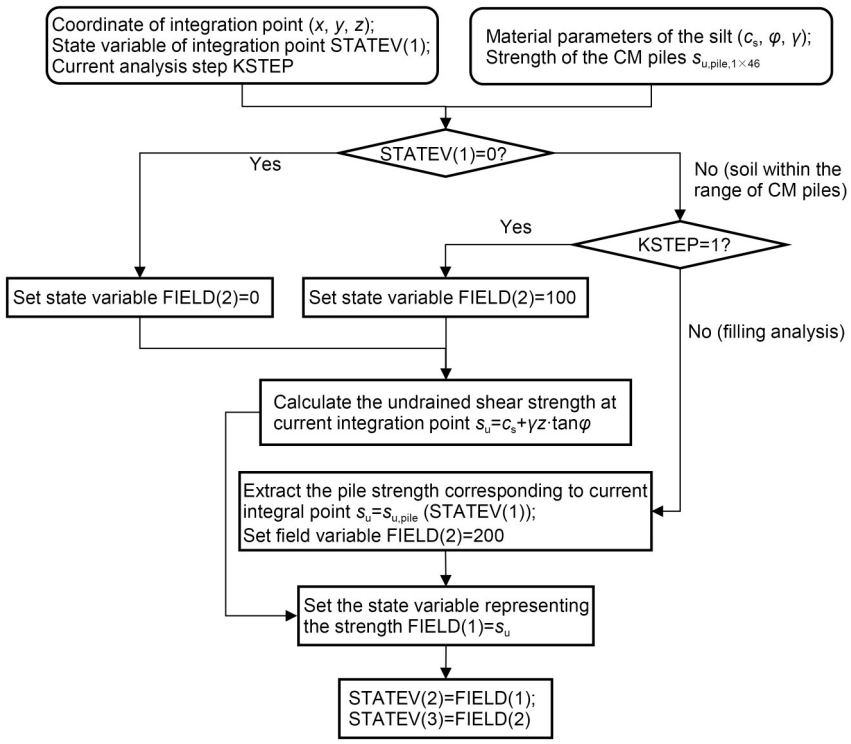

Fig. 12 Flow chart for the USDFLD subroutine

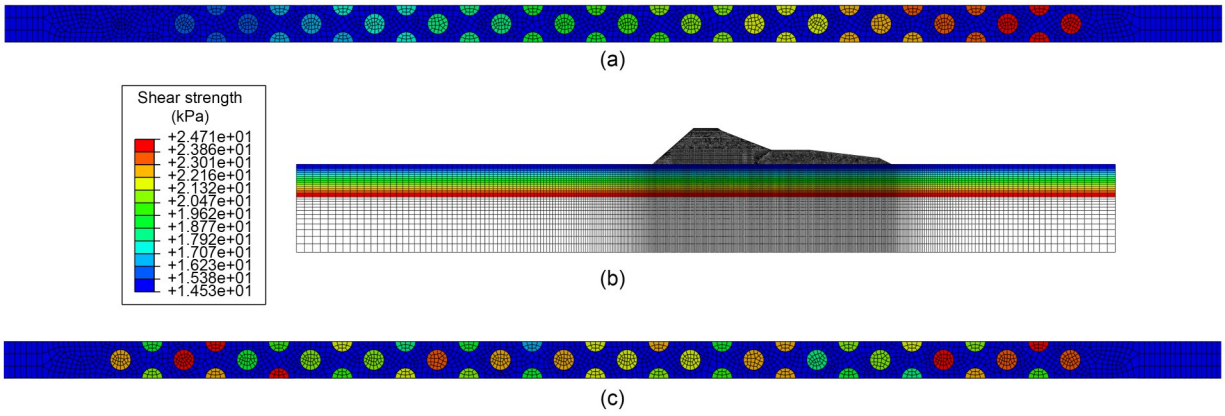

Fig. 13 Values of the state variables and assigned strength field in different analysis steps: (a) state variable STATEV(1) of the foundation soil and the CM piles; (b) strength field STATEV(2) assigned during geo-balance analysis; (c) random strength field of CM piles during filling analysis. References to color refer to the online version of this figure

at the lower half of the seawall and a U-shaped distribution can be observed. This pattern was caused because on the one hand, due to the settlement process of the seawall, the lower half was continuously moving horizontally, resulting in large tensile stress on the seawall, and on the other hand, the elastic modulus of the CM piles was significantly larger than that of the silt, so the top of the piles had a strong extrusion effect on the sand at the bottom of the seawall. The local failure mode of the seawall can be characterized as the settlement at the top and the lateral extrusion damage at the foot. In the composite foundation, the plastic strain of the CM piles was significantly smaller than that of the in situ soil because the undrained shear strength of the former was obviously larger than that of the latter. Some of the CM piles did not undergo plastic deformation. A circular shear slice can be seen on the seawall and the ground soil, corresponding to the deformation pattern of the seawall above.

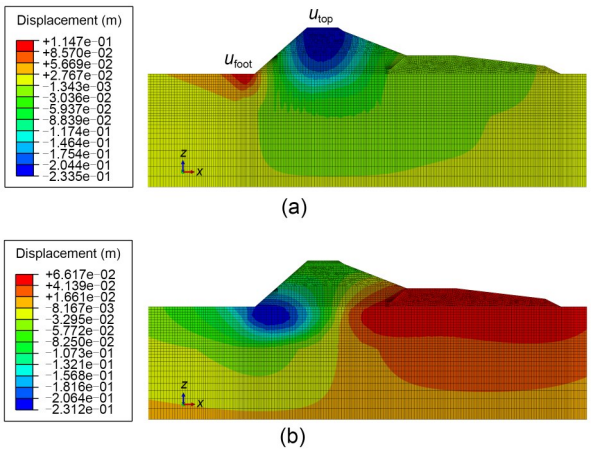

Fig. 14 Displacements of the seawall and ground soil (s_u= 70 kPa, E=500s_u=35.0 MPa): (a) vertical displacement; (b) horizontal displacement. u_{top}: displacement of the top of the seawall; u_{foot}: displacement of the ground soil close to the inner foot of the seawall

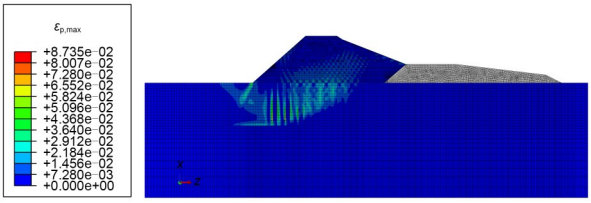

Fig. 15 Distribution of the max principle plastic strain ($\varepsilon_{p,max}$) of the seawall and ground soil (s_u=70 kPa, E=500s_u= 35.0 MPa)

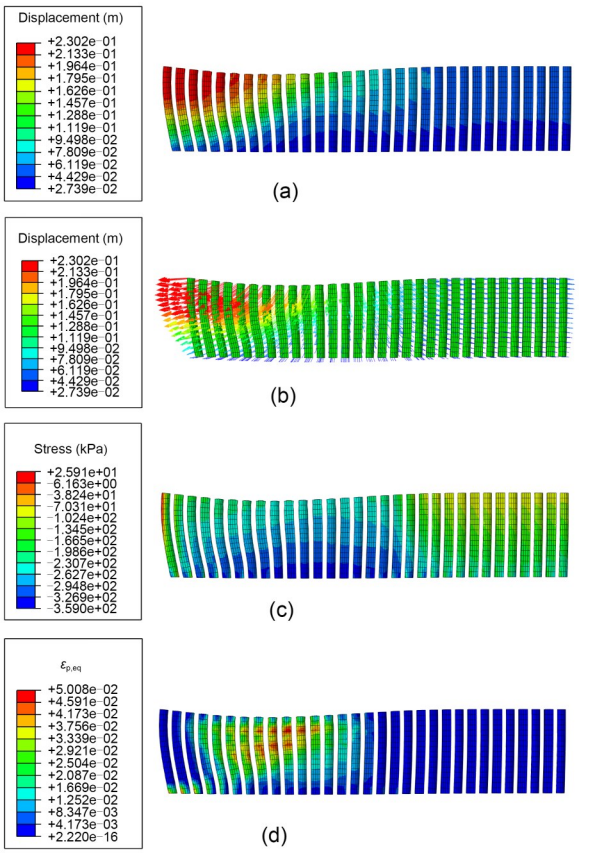

Fig. 16 Response of CM piles: (a) total displacement; (b) illustration of the displacement vector; (c) vertical stress; (d) equivalent plastic strain ($\varepsilon_{p,eq}$)

The displacement pattern, displacement vector, vertical stress, and equivalent plastic strain are shown in Figs. 16a–16d, respectively. Figs. 16a and 16b show that the CM piles close to the inner foot of the seawall exhibited almost exclusively horizontal displacement, and the displacement decreased gradually from the top to the bottom of the CM piles. The closer the CM piles were to the top of the seawall, the more obvious the vertical compression deformation became. Due to the horizontal displacement, the direction of the combined displacement of the pile top was oblique downward to the inner side of the seawall. As shown by Fig. 16c, the vertical compressive stresses on the CM piles directly below the seawall were significantly greater than the rest, with a maximum compressive stress of 359.02 kPa. The innermost CM pile withstood a tensile stress of about 25.91 kPa, owing to the large horizontal displacement at the top of the pile. The plastic strain was also mainly distributed on the cement mixing pile directly beneath the seawall, as shown in Fig. 16d. The maximum equivalent plastic strain was about 5.00×10^{-2}. The plastic strain can also be observed at the bottom of the CM piles close to the inner foot of the seawall, because of the large horizontal displacement at this position.

When the pile strength was taken as s_u=140 kPa and the elastic modulus remained as E=35.0 MPa, the deformation pattern of the seawall was almost the same as that in Fig. 14. The maximum settlement of the top of the seawall was about 14.09 cm. The uplift and the horizontal displacement of the inner foot were approximately 3.78 cm and 11.21 cm, respectively. The results presented above show that the increase in the pile strength reduced the deformation of the seawall and ground soil.

Fig. 17 shows the distribution of plastic strain. The maximum plastic principal strain was about 2.61×10^{-2}, which was only 33.45% of that at s_u=70 kPa. The maximum equivalent plastic strain on the CM piles was about 1.18×10^{-2}, only 23.6% of that at s_u=70 kPa, and the region of plastic strain was also significantly smaller than that calculated at s_u=70 kPa. Due to the

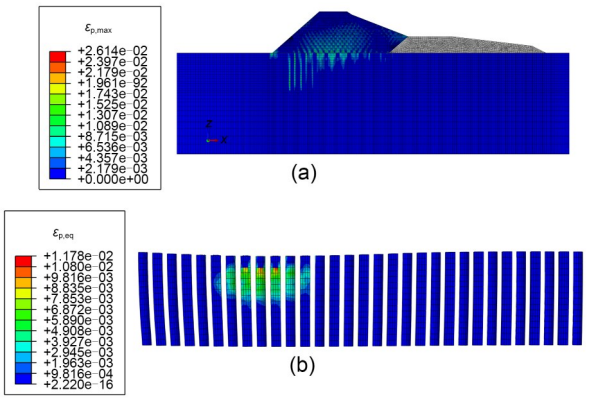

Fig. 17 Plastic response (s_u=140 kPa, E=250s_u=35.0 MPa): (a) distribution of $\varepsilon_{p,max}$ of the seawall and ground soil; (b) $\varepsilon_{p,eq}$ of the CM piles

increase in the strength of the CM piles, the inhibition of the development of plastic strain in the ground soil was significant, and a continuous plastic shear region could no longer be observed. Therefore, it was evident that the stability of the seawall was improved to a great extent.

4.3 Results with random strength among different CM piles

According to the results obtained from the interpolation in Section 3.2, the undrained shear strength of the CM piles followed a normal distribution with a mean value of 144.27 kPa and a coefficient of variation of 0.211. The subroutine described in Fig. 12 was applied to assign the corresponding strength parameters to each CM pile, and Young's modulus of the CM piles was set as 250s_u for simulation; we also performed a statistical analysis.

A total number of 110 samples were calculated, and Fig. 18 shows the results for 100 completed samples; the other 10 samples failed to converge in numerical analysis. The scatter points in Fig. 18 represent the total displacements of the top of the seawall (u_{top}) and the ground soil close to the inner foot of the seawall (u_{foot}) with a certain set of random strengths. We also performed linear regression on the scatter points. The histograms with a fit curve at the top and right represent the probability distribution of the total displacement, which can be regarded as the probability density function when using the normalized axes. From the calculation results, it was apparent that there was an approximately linear relationship between u_{top} and u_{foot}. This is because the potential sliding surface of the seawall is usually close to the circular arc, and the characteristic nodes selected in this study were all within the range of the sliding soil. Therefore, the ratio between u_{top} and u_{foot} was equal to the ratio of the distance between them and the center of the circle of the sliding surface.

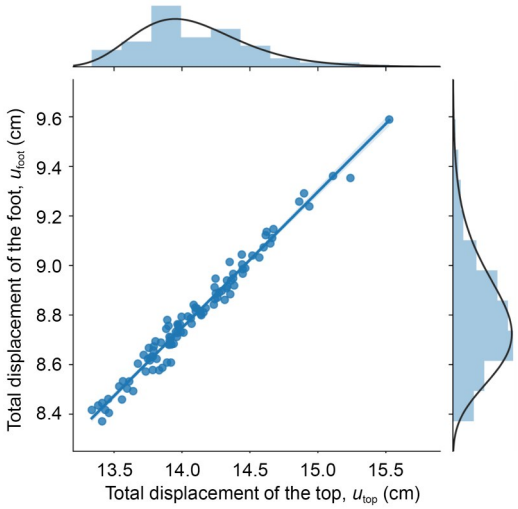

Fig. 18 Total displacement at the top of the seawall and the ground soil close to its foot (E=250s_u)

Due to the uncertainty of the undrained strength of the CM piles, u_{top} and u_{foot} showed a certain degree of discreteness, which could be well fitted by a log-normal distribution. However, the variation intervals of u_{top} and u_{foot} did not exceed 2.5 cm and 1.5 cm, respectively, for the completed samples. The CM piles beneath the seawall were quite dense and the area replacement ratio was large, which significantly improved the overall stiffness of the ground soil, and the tensile effect of the geomembrane bags also effectively limited the displacement of the seawall.

Therefore, we took into consideration the possibility that the moisture content of the ground soil beneath a certain section of the seawall would be higher than the preset average value of 65% due to the field conditions, or that the cement content of the CM piles of a certain section would not reach the preset average value of 14% due to construction conditions, leading to low strength of most of the CM piles. Parametric studies were carried out for the mean values of the cement content μ_{a_c} and the in situ soil moisture content μ_w. The method described in Section 3 was used to determine the distribution of the 24 h undrained shear strength of the CM piles for a specific pair of

(μ_{a_c}, μ_w). Since the amount of deformation of the seawall with each random strength set was similar, for each specific (μ_{a_c}, μ_w) pair, we only completed 20 samples for the sake of computational efficiency. Table 6 provides the values of μ_{a_c} and μ_w involved in the following analysis.

Table 6 Mean values of cement content and moisture content included in analysis

Mean value of cement content, μ_{a_c} (%)	Mean value of in situ moisture content, μ_w (%)
8, 10, 12, 14	65, 70, 75

The calculation results with each (μ_{a_c}, μ_w) pair are summarized in Table 7. Fig. 19 shows the trend of the total displacements at the top of the seawall and the ground soil close to the foot of the seawall with various (μ_{a_c}, μ_w) pairs. A decrease in the cement content and an increase in the moisture content of the in situ soil, which lead to the decrease of the mean value of undrained shear strength of the CM piles, can cause an increase in the mean values of horizontal displacement, vertical displacement, and total displacement of the seawall. Taking the mean value of the displacement with (μ_{a_c}, μ_w) = (14%, 65%) as a standard value, when (μ_{a_c}, μ_w) = (8%, 70%), the total displacement of the top of the seawall was 1.87 times the standard value, and the horizontal and vertical displacements were 3.11 times and 1.81 times the standard value, respectively. For the soil close to the foot of the seawall, the total displacement, horizontal displacement, and vertical displacement were 2.28 times, 2.15 times, and 2.76 times the standard value, respectively. The uncertainty of the overall strength of the CM piles due to quality of construction or field factors can significantly affect the deformation of the seawall and the ground soil.

Meanwhile, when the mean values (μ_{a_c}, μ_w)=(8%, 75%), none of the numerical models converged. The development of the plastic shear region in the last incremental step was similar to that shown in Fig. 15. Consecutive plastic shear zones could be observed, and the plastic strain was more significant. By inference, when the average value of the strength of the CM piles in a certain section of a seawall is below a certain threshold due to the construction quality or the field factors, there will be a risk of overall instability of the seawall. The failure mode can be described as a sliding surface passing through the CM piles under the seawall, giving rise to an excessive displacement of the structure, which seriously affects construction safety.

5 Further discussion

In reality, ground improved by jet grouting and deep mixing has a strongly columnar structure (Nakagawa et al., 1996; Liu et al., 2015) and exhibits significant heterogeneity of cement soil strength within an individual CM pile. This phenomenon has been observed and confirmed in field practice (Chen et al., 2011). Here, we will discuss it further based on the

Table 7 Mean values of displacements with various (μ_{a_c}, μ_w) pairs

μ_{a_c} (%)	μ_w (%)	Top of the seawall			Foundation soil close to the foot		
		Total displacement, u (cm)	Horizontal displacement, u_x (cm)	Vertical displacement, u_z (cm)	Total displacement, u (cm)	Horizontal displacement, u_x (cm)	Vertical displacement, u_z (cm)
8	65	24.402	−7.010	−23.372	17.598	−15.307	8.682
	70	26.394	−8.132	−25.111	20.061	−17.187	10.347
	75	–	–	–	–	–	–
10	65	17.713	−3.791	−17.302	11.251	−10.220	4.707
	70	19.186	−4.277	−18.699	12.166	−11.020	5.156
	75	20.423	−5.156	−19.762	13.138	−11.836	5.703
12	65	14.936	−2.728	−14.683	9.377	−8.501	3.957
	70	16.463	−3.425	−16.098	10.325	−9.381	4.314
	75	17.978	−4.210	−17.470	11.333	−10.291	4.747
14	65	14.092	−2.613	−13.846	8.798	−7.964	3.738
	70	15.100	−3.018	−14.794	9.454	−8.576	3.981
	75	15.550	−3.075	−15.242	9.766	−8.863	4.101

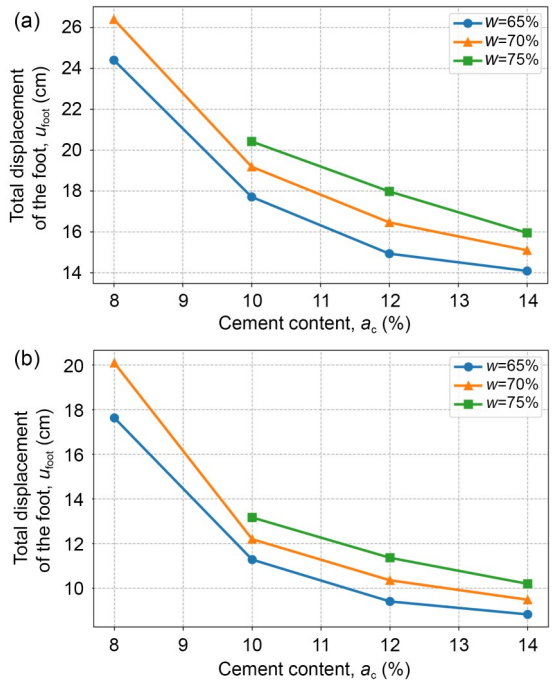

Fig. 19 Total displacements with various pairs of the mean values (μ_{a_c}, μ_w) at the top of the seawall (a) and at the ground soil close to the foot of the seawall (b)

model proposed above, with the aim of providing a deeper and broader reliability analysis of this issue.

5.1 Linear decrease in strength

The strength of each individual CM pile was set to decrease linearly in the z direction to a depth based on the mean strength $s_{u,mean}$=$s_{u,pile}$(STATEV(1)) generated by random sampling, as in Section 4.3. This is illustrated by the following equation:

$$s_u(z) = \frac{6}{5} s_{u,mean} + \frac{1}{20} s_{u,mean} \cdot z, \quad (7)$$

where the value range of z is 0 to −8 m. The radial strength was simplified to be uniform. The random strength of the CM piles in a typical sample is depicted in Fig. 20; a total number of 115 samples were calculated.

Fig. 21a shows the calculation results for 102 completed samples, and similar conclusions can be drawn to those we drew from calculations that did not take into consideration linear decrease of strength. The total displacements of the seawall u_{ave} in the two models are compared in Fig. 21b. The average displacement with a linear decrease of strength within an individual CM pile is smaller than that without. This can be explained as follows: as shown in Fig. 17b, the plastic strain mainly develops in the upper region of the CM piles beneath the seawall, but the strength distribution within an individual CM pile according to Eq. (7) indicates a higher strength than $s_{u,mean}$ in this region, leading to a smaller displacement.

Furthermore, displacement of the seawall by deterministic analysis, where $s_{u,mean}$ is set to be 144.271 kPa, is presented as u_{det} in Fig. 21b. It is evident from the figure that u_{ave} is larger than u_{det} for both models. This result demonstrates that the uncertainty of the strength of the CM piles is not conducive to deformation control of the seawall, and that a design based on deterministic analysis that assumes homogeneous strength of the CM piles can lead to excessive displacement.

5.2 Random strength with a linear decreasing trend within an individual CM pile

On the basis of the model presented above, a random strength with a linear decreasing trend within an individual CM pile was introduced for analysis. The mean strength $s_{u,mean}$ of each CM pile was set to be

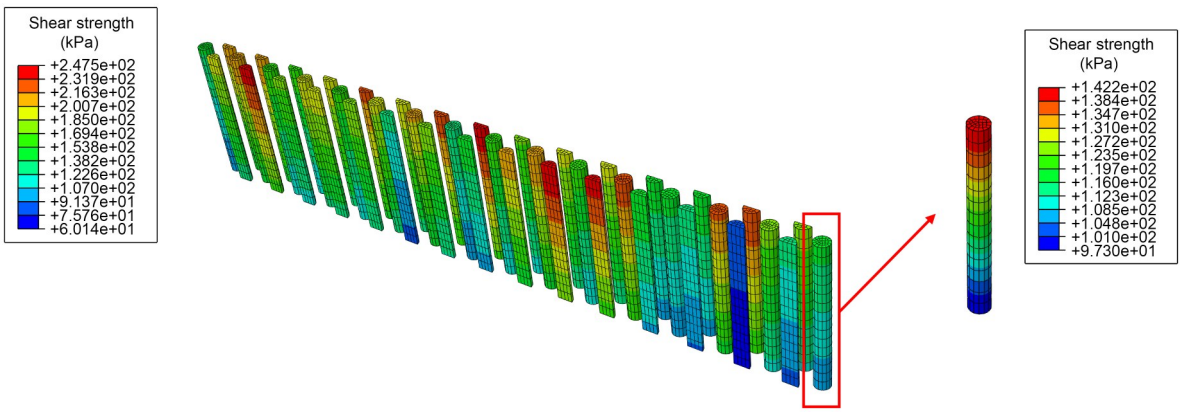

Fig. 20 Random strength of the CM piles in a typical sample

144.271 kPa, while the random strength distribution within an individual CM pile along the z direction was generated by the covariance matrix decomposition method proposed by El-Kadi and Williams (2000); a detailed description is provided in Section S1 of the electronic supplementary materials (ESM). The strength followed a normal distribution and the COV was set to be 0.4 (Larsson, 2005; Chen et al., 2011). The random factor $s_u(z)$ was characterized by an exponential autocorrelation function $\rho_{i,j}$ as Eq. (8) to simultaneously include the spatial correlation:

$$\rho_{i,j}=\exp\left(-\frac{d_{i,j}^{z}}{L_z}\right), \tag{8}$$

where L_z is the correlation distance in the z direction, which is set to be 1 m, and $d_{i,j}^{z}$ is the distance in the z direction between points i and j.

Typical random strength distributions within an individual CM pile are displayed in Fig. 22, and the calculation results for 105 completed samples are presented in Fig. 23. The other 30 samples failed to converge in numerical calculation. The probability of structure failure is calculated to be about 22.2%.

Table 8 presents the convergence rates of three different models for the strength randomness of CM piles. It can be seen that for any group, when the uncertainty of cement soil strength is introduced into the numerical model, there are cases where the model cannot converge. Of the three groups, the one that considers the stochasticity of pile strength within an individual pile shows the most significant probability of instability in the seawall.

Fig. 24 shows the distribution of the shear strength and equivalent plastic strain ($\varepsilon_{p,eq}$) of a failed sample. The results indicate that due to the uncertainty

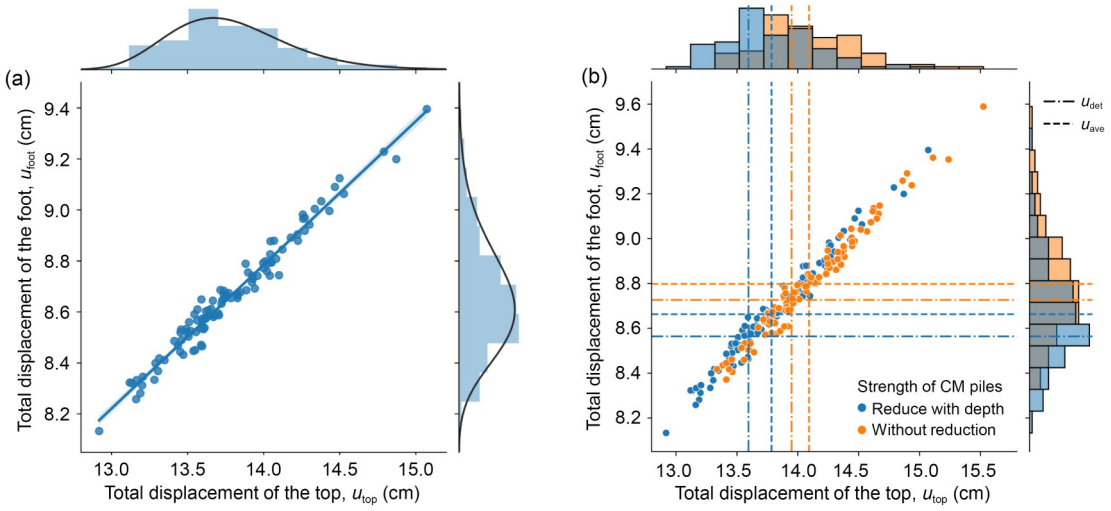

Fig. 21 Calculation results for 102 samples: (a) introducing a linear decrease in strength within an individual CM pile; (b) a comparison between the two models. References to color refer to the online version of this figure

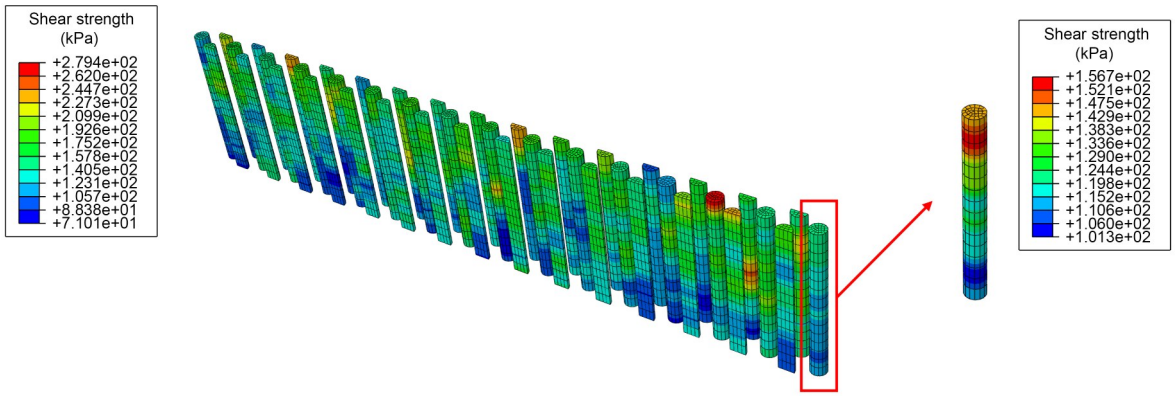

Fig. 22 Typical random strength distributions within an individual CM pile

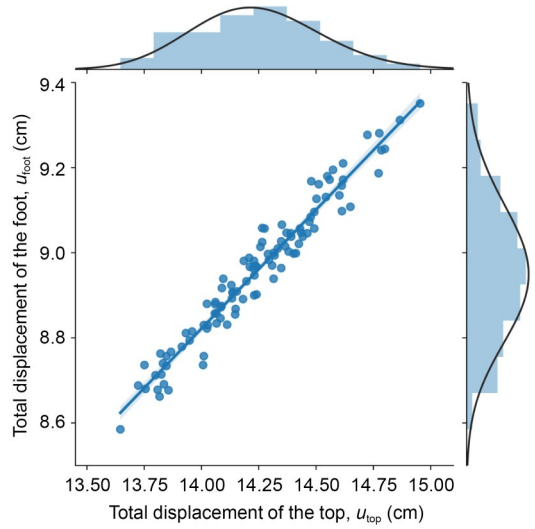

Fig. 23 Distribution of the displacement of completed samples, introducing random strength with a linear decreasing trend

of the strength within an individual CM pile, local plastic strain can develop vigorously in such regions with relatively low undrained shear strength, which leads to non-convergence in numerical models.

The two types of uncertainty are compared in Fig. 25. Obviously, the u_{ave} values of the samples that include the random strength within an individual CM pile are much larger than the u_{det} values, comparing with that introducing the various strengths among each CM pile. This demonstrates that the uncertainty within an individual CM pile has a more significant impact on seawall displacement. In field practice, not only should the variability in strength among different CM piles be carefully controlled, but also the uncertainty of the strength within individual CM piles.

6 Conclusions

A series of vane shear tests have been conducted to investigate the early undrained shear stress of cement-solidified soil curing in seawater. Monte Carlo sampling and 2D bilinear interpolation were used to determine the probability distribution of the 24 h strength of CM piles, using the cement content a_c and the moisture content of the in situ soil w as the random variables. Also, an RFEM method was proposed to obtain the effect of the uncertainty of the strength of CM piles on the deformation and stability of the seawall. Based on the tests and analyses described above, our main conclusions are as follows:

1. With the same curing time, the undrained shear strength of cement soil generally increases with the increase of cement content a_c, but decreases with the increase of in situ soil moisture content w. Within the curing time of this test (24 h), the undrained shear strength of the solidified soil increases significantly with the curing time. Assuming that w and a_c are random variables that follow the normal distribution, the undrained shear strength of the CM piles at 24 h is proven to follow a normal distribution with a mean value of 144.27 kPa and COV of 0.211.

2. Increased strength of CM piles can significantly inhibit the development of plastic strain in both silt and CM piles. The consecutive plastic shear region

Table 8 Convergence rates of three models for the strength randomness of CM piles

Group	Stochasticity of CM pile strength	Convergence rate (%)	Probability of instability (%)
1	Random strength of each CM pile, but uniform within individual piles	90.91	9.09
2	Random average strength of each CM pile, with linear reduction within individual piles	88.70	11.30
3	Fixed average strength, with linear reduction and fluctuation within individual piles	77.78	22.22

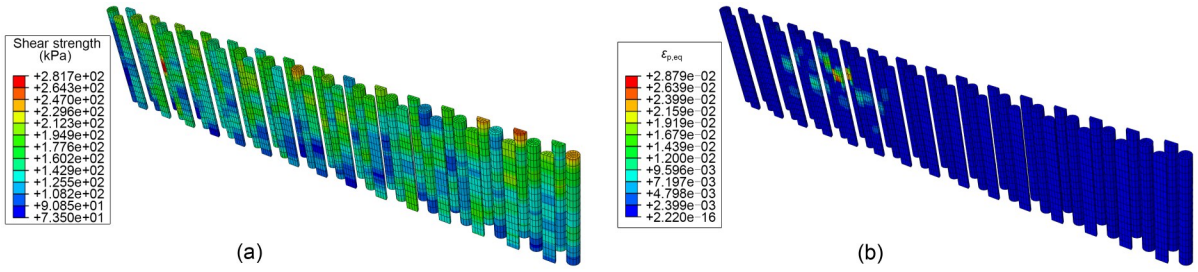

Fig. 24 Distribution of the shear strength (a) and equivalent plastic strain ($\varepsilon_{p,eq}$) (b) of a typical failed sample

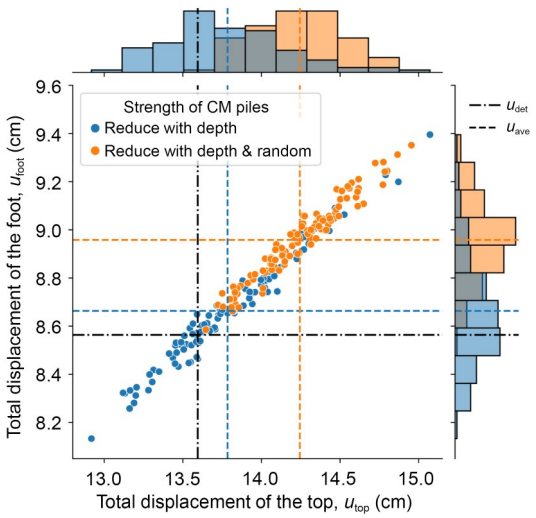

Fig. 25 Comparison between the two types of uncertainty

passing through the ground soil and seawall gradually disappears, and the stability of the seawall is improved.

3. Due to the uncertainty of the undrained strength of CM piles, u_{top} and u_{foot} show a certain degree of discreteness, and can be well fitted by a log-normal distribution. A decrease in cement content and an increase in moisture content of the in situ soil lead to a decrease in the mean value of the undrained shear strength of the CM piles. The mean values of horizontal displacements, vertical displacements, and total displacements of the seawall will increase accordingly. If the mean strength of the CM piles is lower than a certain threshold due to factors such as construction quality or soil properties, there is a high risk of overall instability of the structure.

4. The heterogeneity of strength within an individual CM pile has a more significant impact on the displacement of the seawall. Local plastic strain can develop aggressively in regions with low undrained shear strength, which leads to non-convergence in numerical models. The probability of structure failure is about 22.2%.

In conclusion, when improving ground with CM piles, the uncertainty of the undrained shear strength has a significant impact on deformation and stability of the seawall. Such uncertainty is not conducive to controlling deformation of the seawall, and a design referring to the deterministic analysis can lead to excessive displacement or even structure failure. Not only the strength variability among different CM piles but also the heterogeneity of the strength within an individual CM pile should be controlled carefully.

However, the model proposed in this paper does have some shortcomings. Firstly, we selected the Mohr-Coulomb model to describe the soil behavior, which is challenging to describe the strain-softening behavior exhibited by cement-treated soil due to its structural nature. In future studies, it would be beneficial to consider adopting more complex and accurate constitutive models. Secondly, the use of Monte Carlo simulation-based statistical analysis makes a large number of calculations to obtain a reliable distribution of seawall deformation or safety factor. Moreover, the fine modeling of cement mixing piles leads to a large number of grids, resulting in a huge demand for computational resources in the RFEM model. Our subsequent research will focus on reducing the model's calculation time and improving computational efficiency while ensuring accuracy.

Acknowledgments

This work is supported by the Finance Science and Technology Project of Hainan Province (No. ZDKJ202019), the Key Research and Development Program of Zhejiang Province (No. 2021C03014), and the Natural Science Foundation of Zhejiang Province (No. LR22E080005), China.

Author contributions

Yuansheng YU and Zhen GUO designed the research. Yuansheng YU and Lingling LI processed the corresponding data. Yuansheng YU and Xiangmiao KONG wrote the first draft of the manuscript. Chengyuan LI helped to organize the manuscript. Zhen GUO revised and edited the final version.

Conflict of interest

Yuansheng YU, Lingling LI, Xiangmiao KONG, Chengyuan LI, and Zhen GUO declare that they have no conflict of interest.

References

ABAQUS Inc., 2016. ABAQUS User Subroutines Reference Guide. Dassault Systèmes, Paris, France.

ASTM (American Society for Testing and Materials), 2014. Standard Test Methods for Specific Gravity of Soil Solids by Water Pycnometer, ASTM D854-14. ASTM, West Conshohocken, USA. https://doi.org/10.1520/D0854-14

ASTM (American Society for Testing and Materials), 2016. Standard Test Methods for Laboratory Miniature Vane Shear Test for Saturated Fine-Grained Clayey Soil, ASTM D4648M-16. ASTM, West Conshohocken, USA. https://doi.org/10.1520/D4648_D4648M-16

ASTM (American Society for Testing and Materials), 2018. Standard Test Methods for Liquid Limit, Plastic Limit,

and Plasticity Index of Soils, ASTM D4318-17. ASTM, West Conshohocken, USA. https://doi.org/10.1520/D4318-17

ASTM (American Society for Testing and Materials), 2019. Standard Test Methods for Laboratory Determination of Water (Moisture) Content of Soil and Rock by Mass, ASTM D2216-19. ASTM, West Conshohocken, USA. https://doi.org/10.1520/D2216-19

ASTM (American Society for Testing and Materials), 2021. Standard Test Methods for Laboratory Determination of Density and Unit Weight of Soil Specimens, ASTM D7263-21. ASTM, West Conshohocken, USA. https://doi.org/10.1520/D7263-21

Cassidy MJ, Uzielli M, Tian YH, 2013. Probabilistic combined loading failure envelopes of a strip footing on spatially variable soil. *Computers and Geotechnics*, 49:191-205. https://doi.org/10.1016/j.compgeo.2012.10.008

Chai JC, Shrestha S, Hino T, et al., 2015. 2D and 3D analyses of an embankment on clay improved by soil–cement columns. *Computers and Geotechnics*, 68:28-37. https://doi.org/10.1016/j.compgeo.2015.03.014

Chen J, Lee FH, Ng CC, 2011. Statistical analysis for strength variation of deep mixing columns in Singapore. *In*: Han J, Alzamora DA (Eds.), Geo-Frontiers 2011: Advances in Geotechnical Engineering. American Society of Civil Engineers, Reston, USA, p.576-584. https://doi.org/10.1061/41165(397)60

der Kiureghian A, Ditlevsen O, 2009. Aleatory or epistemic? Does it matter? *Structural Safety*, 31(2):105-112. https://doi.org/10.1016/j.strusafe.2008.06.020

El-Kadi AI, Williams SA, 2000. Generating two-dimensional fields of autocorrelated, normally distributed parameters by the matrix decomposition technique. *Groundwater*, 38(4):530-532. https://doi.org/10.1111/j.1745-6584.2000.tb00245.x

Fenton GA, Griffiths DV, 2008. Risk Assessment in Geotechnical Engineering. John Wiley & Sons, Hoboken, USA. https://doi.org/10.1002/9780470284704

Garzón LX, Caicedo B, Sánchez-Silva M, et al., 2015. Physical modelling of soil uncertainty. *International Journal of Physical Modelling in Geotechnics*, 15(1):19-34. https://doi.org/10.1680/ijpmg.14.00012

Griffiths DV, Fenton GA, 2009. Probabilistic settlement analysis by stochastic and random finite-element methods. *Journal of Geotechnical and Geoenvironmental Engineering*, 135(11):1629-1637. https://doi.org/10.1061/(ASCE)GT.1943-5606.0000126

Horpibulsk S, Rachan R, Suddeepong A, et al., 2011. Strength development in cement admixed Bangkok clay: laboratory and field investigations. *Soils and Foundations*, 51(2):239-251. https://doi.org/10.3208/sandf.51.239

Hu LH, Takahashi A, Kasama K, 2022. Effect of spatial variability on stability and failure mechanisms of 3D slope using random limit equilibrium method. *Soils and Foundations*, 62(6):101225. https://doi.org/10.1016/j.sandf.2022.101225

Jamsawang P, Voottipruex P, Boathong P, et al., 2015. Three-dimensional numerical investigation on lateral movement and factor of safety of slopes stabilized with deep cement mixing column rows. *Engineering Geology*, 188:159-167. https://doi.org/10.1016/j.enggeo.2015.01.017

Jamshidi Chenari R, Pourvahedi Roshandeh S, Payan M, 2019. Stochastic analysis of foundation immediate settlement on heterogeneous spatially random soil considering mechanical anisotropy. *SN Applied Sciences*, 1(7):660. https://doi.org/10.1007/s42452-019-0684-0

Jiang SH, Huang JS, 2016. Efficient slope reliability analysis at low-probability levels in spatially variable soils. *Computers and Geotechnics*, 75:18-27. https://doi.org/10.1016/j.compgeo.2016.01.016

Jiang SH, Li DQ, Cao ZJ, et al., 2015. Efficient system reliability analysis of slope stability in spatially variable soils using Monte Carlo simulation. *Journal of Geotechnical and Geoenvironmental Engineering*, 141(2):04014096. https://doi.org/10.1061/(ASCE)GT.1943-5606.0001227

Kamruzzaman AH, Chew SH, Lee FH, 2009. Structuration and destructuration behavior of cement-treated Singapore marine clay. *Journal of Geotechnical and Geoenvironmental Engineering*, 135(4):573-589. https://doi.org/10.1061/(asce)1090-0241(2009)135:4(573)

Kirkland EJ, 2010. Bilinear interpolation. *In*: Kirkland EJ (Ed.), Advanced Computing in Electron Microscopy. 2nd Edition. Springer, New York, USA, p.261-263. https://doi.org/10.1007/978-1-4419-6533-2_12

Kitazume M, Nakamura T, Terashi M, et al., 2003. Laboratory tests on long-term strength of cement treated soil. *In*: Johnsen L, Bruce DA, Byle MJ, et al. (Eds.), Grouting and Ground Treatment. American Society of Civil Engineers, Reston, USA, p.586-597. https://doi.org/10.1061/40663(2003)31

Lacasse S, Nadim F, 1996. Uncertainties in characterising soil properties. *In*: Shackleford CD, Nelson PP, Roth MJS (Eds.), Uncertainty in the Geologic Environment: from Theory to Practice. American Society of Civil Engineers, New York, USA, p.49-75.

Larsson S, 2005. State of practice report–execution, monitoring and quality control. Proceedings of the International Conference on Deep Mixing Best Practice and Recent Advances–Deep Mixing, p.732-785.

Li DQ, Zheng D, Cao ZJ, et al., 2016. Response surface methods for slope reliability analysis: review and comparison. *Engineering Geology*, 203:3-14. https://doi.org/10.1016/j.enggeo.2015.09.003

Li JH, Zhou Y, Zhang LL, et al., 2016. Random finite element method for spudcan foundations in spatially variable soils. *Engineering Geology*, 205:146-155. https://doi.org/10.1016/j.enggeo.2015.12.019

Li L, Li JH, Huang JS, et al., 2017a. The bearing capacity of spudcan foundations under combined loading in spatially variable soils. *Engineering Geology*, 227:139-148. https://doi.org/10.1016/j.enggeo.2017.03.022

Li L, Li JH, Huang JS, et al., 2017b. Bearing capacity of spudcan foundations in a spatially varying clayey seabed. *Ocean Engineering*, 143:97-105.

https://doi.org/10.1016/j.oceaneng.2017.05.026

Liu Y, Lee FH, Quek ST, et al., 2015. Effect of spatial variation of strength and modulus on the lateral compression response of cement-admixed clay slab. *Géotechnique*, 65(10):851-865. https://doi.org/10.1680/jgeot.14.P.254

Lu WH, Miao LC, 2015. A simplified 2-D evaluation method of the arching effect for geosynthetic-reinforced and pile-supported embankments. *Computers and Geotechnics*, 65: 97-103. https://doi.org/10.1016/j.compgeo.2014.11.014

Metropolis N, Ulam S, 1949. The Monte Carlo method. *Journal of the American Statistical Association*, 44:335-341. https://doi.org/10.1080/01621459.1949.10483310

Nakagawa S, Kamegaya L, Kureha K, et al., 1996. Case history and behavioural analyses of braced large scale open excavation in very soft reclaimed land in coastal area. The International Symposium on Geotechnical Aspects of Underground Construction in Soft Ground, p.179-184.

Nunez MA, Briançon L, Dias D, 2013. Analyses of a pile-supported embankment over soft clay: full-scale experiment, analytical and numerical approaches. *Engineering Geology*, 153:53-67. https://doi.org/10.1016/j.enggeo.2012.11.006

Vanmarcke EH, 1977. Probabilistic modeling of soil profiles. *Journal of the Geotechnical Engineering Division*, 103(11): 1227-1246. https://doi.org/10.1061/AJGEB6.0000517

Wu CL, Li JH, Liu JC, 2022. Experimental study of a shallow foundation on spatially variable soils. *Georisk: Assessment and Management of Risk for Engineered Systems and Geohazards*, 16(2):225-234. https://doi.org/10.1080/17499518.2020.1806333

Wu YX, Zhang HL, Shu S, 2022. Probabilistic bearing capacity of spudcan foundations under combined loading in spatially variable soils. *Ocean Engineering*, 248:110738. https://doi.org/10.1016/j.oceaneng.2022.110738

Zhu D, Griffiths DV, Huang J, et al., 2017. Probabilistic stability analyses of undrained slopes with linearly increasing mean strength. *Géotechnique*, 67(8):733-746. https://doi.org/10.1680/jgeot.16.P.223

Electronic supplementary materials

Section S1